



Microscopic Tunneling Model of Nb–AlN–NbN Josephson Flux-Flow Oscillator

D. R. Gulevich¹ · L. V. Filippenko² · V. P. Koshelets²

Received: 28 August 2018 / Accepted: 25 November 2018
© Springer Science+Business Media, LLC, part of Springer Nature 2018

Abstract

Since the very first experimental realization of a Josephson flux-flow oscillator (FFO), its theoretical description has been limited by the phenomenological perturbed sine-Gordon equation (PSGE). While PSGE can qualitatively describe the topological excitations in Josephson junctions that are sine-Gordon solitons or fluxons, it is unable to capture essential physical phenomena of a realistic system such as the coupling between tunnel currents and electromagnetic radiation. Furthermore, PSGE neglects any dependence on energy gaps of superconductors and makes no distinction between symmetric and asymmetric junctions: those made of two identical or two different superconducting materials. It was not until recently when it became possible to calculate properties of FFO by taking into account information about energy gaps of superconductors (Gulevich et al. in *Phys Rev B* 96:024215, 2017). Such approach is based on the microscopic tunneling theory and has been shown to describe essential features of symmetric Nb–AlO_x–Nb junctions. Here, we extend this approach to asymmetric Nb–AlN–NbN junctions and compare the calculated current–voltage characteristics to our experimental results.

Keywords Microscopic tunneling theory · Flux-flow oscillator · Nb–AlN–NbN contacts · Tunnel current amplitudes · Josephson self-coupling

1 Introduction

Nb-based tunnel junctions are basic elements in most of the devices and circuits of low-temperature superconducting electronics [1]. Nb–AlO_x–Nb junctions are successfully used in SQUIDS [2–4], RSFQ (rapid single flux quantum) digital circuits [5,6] and

✉ D. R. Gulevich
d.r.gulevich@metalab.ifmo.ru

¹ ITMO University, St. Petersburg, Russia 197101

² Kotelnikov Institute of Radio Engineering and Electronics, Russian Academy of Science, Moscow, Russia 125009

quantum computing [7–9]. Because the noise temperature of SIS mixers is limited only by the fundamental quantum value $hf/2k_B$ [10–13], superconductor–insulator–superconductor (SIS) mixers that employ high-quality Nb-based tunnel junctions are used in the most advanced space and ground-based mm- and submm-range radio telescopes. The widespread use of the Nb–AlO_x–Nb tunnel junctions owes to the fact that a very thin Al layer can completely cover the base Nb electrode [14–16] while compensating the surface roughness of the Nb film, yielding a very high-quality tunnel barrier.

To realize a quantum-limited performance at frequencies of about 1 THz, SIS tunnel junctions with high current density, high energy gap and extremely small leakage currents are required. However, there exists a limit for increasing of the AlO_x barrier transparency: At values of the current density higher than about 10–15 kA/cm², an abrupt degradation of the junction quality takes place. The idea of utilizing SIS tunnel junctions for heterodyne mixing at THz frequencies has received a remarkable support due to the development of Nb–AlN–Nb tunnel junctions with very high current densities up to 100 kA/cm² [17–22]. This corresponds to low $R_N S$ values down to $2 \Omega \mu\text{m}^2$ (R_N and S are the normal state resistance and area of the SIS junction, respectively). AlN tunnel barrier in combination with a top superconducting NbN electrode provides a significant improvement in the quality of the SIS junction at high current density [22,23]. In this case, the ratio of subgap and normal state resistances R_J/R_N , which characterizes quality of the tunnel barrier, becomes substantially enhanced. The R_J/R_N ratio as high as 28 was realized for Nb–AlN–NbN junctions at tunnel current density 20 kA/cm². This value exceeds by far those for Nb–AlN–Nb ($R_J/R_N = 16$) and Nb–AlO_x–Nb ($R_J/R_N = 7$) junctions, at the same current density [23]. Along with low leakage current, the Nb–AlN–NbN junctions provide high energy gap voltage V_g up to 3.7 mV, which extends considerably the operation range of SIS mixers at frequencies of around 1 THz [24].

High-quality Nb–AlN–NbN tunnel junctions were successfully used for development of Josephson flux-flow oscillator (FFO) [25] which serves as a local oscillator in fully integrated superconducting receivers [26,27]. Higher gap voltage of Nb–AlN–NbN junctions as compared to Nb–AlO_x–Nb results in higher Josephson self-coupling voltage $V_{JSC} = V_g/3$ [28] (620 GHz for the Nb–AlN–NbN junctions versus 450 GHz for Nb–AlO_x–Nb in frequency units), which provides an opportunity to engineer junction properties to suit the imposed requirements to a local oscillator.

Despite the success in fabrication and use of Nb–AlN–NbN FFO, theory of these systems remains far from being developed. Most of the theoretical studies of FFO so far were based on the perturbed sine-Gordon equation (PSGE) which does not use any information about the material and, therefore, is unable to provide an adequate description of realistic devices. This paper aims to fill this gap by providing a theoretical description of Nb–AlN–NbN FFO from the perspective of the microscopic tunneling theory (MTT) [29,30].

2 Microscopic Tunneling Model of FFO

FFO was proposed in 1983 [25], and it took years of research before a practical system was developed [31]. The reliability of FFO as a local oscillator in high-resolution heterodyne spectrometers [32] has been verified in field, in studies of the Earth atmosphere [26,33], and in the laboratory, in measurements of radiation emitted from BSCCO intrinsic Josephson junction stacks [27,34]. Despite the FFO being a subject of many theoretical studies [35–54], its description has been largely limited by the PSGE. The PSGE is a phenomenological theory whose treatment of the superconducting and quasiparticle tunnel currents is only justified in a static (i.e., low-frequency) limit and close to the critical temperature [55]: conditions which are rarely satisfied in practical systems. Furthermore, PSGE does not use any information about energy gaps of the constituting materials which is particularly essential for systems operating in the high-frequency regime. Recently, we have initiated an approach to theoretical description of FFO based on the MTT [29,30] and applied it to the description of symmetric Nb–AlO_x–Nb junctions [56]. The study yielded development of the MiT-MoJCo code (Microscopic Tunneling Model for Josephson Contacts) [57,58]. Below, we will extend this approach to a more general case of asymmetric junctions made of different superconducting materials, such as Nb–AlN–NbN.

In the study of Nb–AlO_x–Nb FFO [56], it was shown that coupling to the SIS detector makes little or no effect to the shape of current–voltage characteristics (IVC) of FFOs. As in this paper we are mainly interested in the effect of finite superconducting energy gaps of two superconductors on the shape of IVC, here we neglect the contribution of the load and assume the FFO radiation end is unloaded. Then, in normalized units, the quasi-one-dimensional microscopic model of FFO of width profile $W(x)$, see Fig. 1 and Ref. [56],

$$\varphi_{tt} - \left(1 + \beta \frac{\partial}{\partial t}\right) \varphi_{xx} - \frac{W'(x)}{W(x)} \left[h_{\text{ext}} + \left(1 + \beta \frac{\partial}{\partial t}\right) \varphi_x \right] + j(x, t) - \Gamma_{\text{eff}}(x) = 0, \quad (1)$$

$$j(x, t) = \frac{k}{\text{Re } \tilde{j}_p(0)} \int_0^\infty \left\{ j_p(kt') \sin \left[\frac{\varphi(x, t) + \varphi(x, t - t')}{2} \right] + j_{qp}(kt') \sin \left[\frac{\varphi(x, t) - \varphi(x, t - t')}{2} \right] \right\} dt' \quad (2)$$

and the superconducting phase difference $\varphi(x, t)$ satisfies boundary conditions at the FFO’s ends

$$\varphi_x(\pm L/2, t) = -h_{\text{ext}}. \quad (3)$$

Here, L and $W(x)$ are the normalized length and width of the junction, respectively, $k = \omega_g/\omega_J$ is ratio of the gap and Josephson plasma frequencies, β is the surface damping parameter and h_{ext} is the normalized external magnetic field in units $j_c \lambda_J$, where j_c is the critical current density and λ_J is the Josephson penetration length. Assuming a the junction layout is symmetric with respect to the x axis (see Fig. 1),

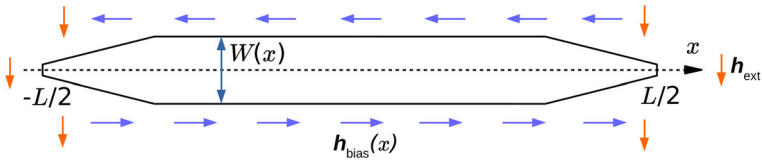


Fig. 1 Sketch of a typical geometry of Josephson flux-flow oscillator used as a radiation source in a superconducting integrated receiver [23]. The length and width of the junction are not in scale: The experimental sample studied in this paper was designed with a length $L = 400 \mu\text{m}$ and width $W(x) = 16 \mu\text{m}$ for $|x| < 160 \mu\text{m}$, decreasing linearly to $W(\pm L/2) = 1 \mu\text{m}$ at the edges. In the experimental setup, the magnetic fields $h_{\text{bias}}(x)$ and h_{ext} were induced by the bias current I passing through the junction and the current in a dedicated control line I_{CL} , respectively (Color figure online)

the effective bias current equals

$$\Gamma_{\text{eff}}(x) = \frac{2h_{\text{bias}}(x)}{W(x)}, \tag{4}$$

where $h_{\text{bias}}(x)$ is magnitude of the normalized magnetic field induced by the bias current along x . The spatial profile of the effective bias current $h_{\text{bias}}(x)$ is not known precisely as it depends on the electromagnetic environment in presence of all electrodes and circuitry. For a comprehensive numerical modeling, it can be determined by a full electromagnetic calculation using the specialized software [48,59–61]. In this paper, we resort to a simple model where $h_{\text{bias}}(x)$ is taken constant. The justification for this is that while in a long superconducting strip the current rises toward the edges as $\sim 1/\sqrt{\Delta x}$ [62], where Δx is the distance from the strip edge, in real systems the width of the electrodes connected to the FFO is typically made smaller than the length of FFO to compensate for this rise.

Real-valued time-domain kernels $j_p(\tau)$ and $j_{qp}(\tau)$ satisfy the causality condition

$$j_{p,qp}(\tau) = 0 \quad \text{for } \tau < 0 \tag{5}$$

and are connected to the complex quantities $\tilde{j}_p(\xi)$ and $\tilde{j}_{qp}(\xi)$ in the frequency domain by the inverse Fourier transforms [56],

$$\begin{aligned} j_p(\tau) &= \frac{1}{2\pi} \int_{-\infty}^{\infty} \tilde{j}_p(\xi) e^{i\xi\tau} d\xi \\ j_{qp}(\tau) &= \frac{1}{2\pi} \int_{-\infty}^{\infty} \tilde{j}_{qp}(\xi) e^{-i\xi\tau} d\xi. \end{aligned} \tag{6}$$

Note the difference of the two different sign conventions of Fourier transforms which is kept for historical reasons (see note [54] in Ref. [56]). Because $j_{p,qp}(\tau)$ are real, the transformed quantities satisfy $\tilde{j}_{p,qp}(-\xi) = \tilde{j}_{p,qp}^*(\xi)$, and, as a consequence of the causality (5), their real and imaginary parts are connected by dispersion relations of the Kramers–Kronig type [63,64]. The complex functions $\tilde{j}_p(\xi)$ and $\tilde{j}_{qp}(\xi)$ are referred to as tunnel current amplitudes (TCAs). The following three sections will be devoted to determination of TCAs for Nb–AlN–NbN junctions.

3 Tunnel Current Amplitudes for Nb–AlN–NbN Junction

Expressions for TCAs were derived from the Bardeen–Cooper–Schrieffer (BCS) theory by Larkin and Ovchinnikov [30]. For a Josephson junction formed by superconductors with gaps $\delta_1 \equiv \Delta_1/\hbar\omega_g$ and $\delta_2 \equiv \Delta_2/\hbar\omega_g$ normalized to $\hbar\omega_g \equiv \Delta_1 + \Delta_2$ these expressions are summarized in Appendix of Ref. [56]. (We refer readers to the verified expressions in Ref. [56] because the original expressions of Larkin and Ovchinnikov were given with a misprint.) The BCS predictions differ slightly from experimental observations: In Nb junctions, smaller critical current densities are observed, while the logarithmic singularities (Riedel peaks) are smeared by several competing mechanisms [55,64]. To compensate these deficiencies, phenomenological corrections are applied to the BCS results, that is, (i) smoothing the Riedel peaks and (ii) renormalizing the pair current density.

We correct bare BCS TCAs introducing a phenomenological peak width 2δ and using the smoothing procedure which conserves the Kramers–Kronig transforms. For an asymmetric junction with $\delta_1 \neq \delta_2$, assuming $0 < \delta_2 - \delta_1 \equiv \delta_{21}$, the smoothing procedure takes the form [64],

$$\begin{aligned} \operatorname{Re} \tilde{j}_{p,qp}(\xi) \rightarrow \operatorname{Re} \tilde{j}_{p,qp}(\xi) \pm \frac{\pi \xi \sqrt{\delta_1 \delta_2}}{8\delta_{21}} [\tanh(\alpha\delta_2) - \tanh(\alpha\delta_1)] \\ \times \left[\frac{2}{\pi} \arctan \frac{(\xi - \delta_{21})}{\delta} - \operatorname{sgn}(\xi - \delta_{21}) + \frac{2}{\pi} \arctan \frac{(\xi + \delta_{21})}{\delta} - \operatorname{sgn}(\xi + \delta_{21}) \right] \\ - \frac{\xi \operatorname{Re} \tilde{j}_p(0)}{2\pi} \ln \left\{ \frac{[(1 - \xi)^2 + \delta^2](1 + \xi)^2}{(1 - \xi)^2[(1 + \xi)^2 + \delta^2]} \right\} \end{aligned} \quad (7)$$

$$\begin{aligned} \operatorname{Im} \tilde{j}_{p,qp}(\xi) \rightarrow \operatorname{Im} \tilde{j}_{p,qp}(\xi) - \frac{\xi \sqrt{\delta_1 \delta_2}}{8\delta_{21}} [\tanh(\alpha\delta_2) - \tanh(\alpha\delta_1)] \\ \times \ln \left\{ \frac{[(\xi - \delta_{21})^2 + \delta^2][(\xi + \delta_{21})^2 + \delta^2]}{(\xi - \delta_{21})^2(\xi + \delta_{21})^2} \right\} \\ \pm \frac{\xi \operatorname{Re} \tilde{j}_p(0)}{2} \left[\frac{2}{\pi} \arctan \frac{(1 - \xi)}{\delta} - \operatorname{sgn}(1 - \xi) \right. \\ \left. + \frac{2}{\pi} \arctan \frac{(1 + \xi)}{\delta} - \operatorname{sgn}(1 + \xi) \right], \end{aligned} \quad (8)$$

where the plus and minus signs in Eqs. (7) and (8) correspond to the pair and quasi-particle currents, respectively, and the parameter $\alpha = \hbar\omega_g/2k_B T$ incorporates the dependence on temperature T .

The value of the phenomenological smoothing parameter δ which enters (7) and (8) can be determined from the experiments. In Ref. [56], we used IVC of voltage-biased SIS mixer made using the same technology as the FFO to determine the optimal parameter δ for the Riedel peak smoothness. As we will show in the next sections, this parameter can also be obtained directly from the IVC of FFO.

The pair current correction is implemented by performing a replacement

$$\tilde{j}_p(\xi) \rightarrow \alpha_{\text{supp}} \tilde{j}_p(\xi) \quad (9)$$

with the suppression parameter $\alpha_{\text{supp}} < 1$ and leaving intact the quasiparticle component $\tilde{j}_{qp}(\xi)$.

4 FFO in Large Magnetic Field Limit

In large magnetic fields,¹ the Josephson effect in the junction becomes suppressed² and its dynamics becomes determined predominantly by the quasiparticle current. In this regime, the theoretical description of FFO becomes particularly simple and enables to derive analytical formulas.

To simplify the theoretical analysis, consider a FFO of constant width $W'(x) = 0$ and neglect the surface damping $\beta = 0$,

$$\varphi_{tt} - \varphi_{xx} + j(x, t) - \gamma = 0, \quad \varphi_x(\pm L/2, t) = -h_{\text{ext}}, \quad (10)$$

where $\gamma = I/I_c$ and $j(x, t)$ is given by expression (2). Consider the limit of a very high magnetic field $h_{\text{ext}} \gg 1$. In a steady state, the superconducting phase difference can be taken in the form

$$\varphi(x, t) \approx 2 v_{dc} t - h_{\text{ext}} x, \quad (11)$$

where v_{dc} is the normalized dc voltage in units $\hbar\omega_J/e$ and the terms neglected in (11) are of the order $O(1/h_{\text{ext}}^2)$. Substituting (11) to (10) and taking the time average, we get

$$\gamma = \frac{k}{\text{Re } \tilde{j}_p(0)} \int_0^\infty j_{qp}(kt') \sin v_{dc} t' dt'$$

¹ By “large” magnetic fields, we mean the fields significantly larger than the characteristic magnetic field in the junction, that is, $j_c \lambda_J \sim 3 \times 10^{-4}$ Tesla for our experimental samples. This is significantly smaller than the critical field $H_{c1} \approx 0.14$ Tesla for bulk Nb at $T = 4.2$ K [65]. Given this, we assume that properties of the superconductors such as their energy gaps as well as smearing mechanisms responsible for the Riedel peak smoothing are unaffected by application of the external magnetic field.

² Note that because $j_c \lambda_J \ll H_{c1}$ the Josephson can only be suppressed *integrally* in the junction but not locally. That is, the pair currents are still present in full in any particular point of the Josephson but affect weakly the global dynamics of the junction.

Using the causality properties of the TCAs (5), we can extend the integration to the negative values of t' and write

$$\begin{aligned} \gamma &= \frac{k}{\text{Re } \tilde{j}_p(0)} \int_{-\infty}^{\infty} j_{qp}(kt') \sin v_{dc}t' dt' \\ &= \frac{k}{2\pi \text{Re } \tilde{j}_p(0)} \int_{-\infty}^{\infty} \int_{-\infty}^{\infty} \tilde{j}_{qp}(\xi) e^{-i\xi kt'} \sin v_{dc}t' d\xi dt' \\ &= \frac{1}{\text{Re } \tilde{j}_p(0)} \int_{-\infty}^{\infty} d\xi \tilde{j}_{qp}(\xi) \frac{1}{2i} \left[\delta\left(\xi - \frac{v_{dc}}{k}\right) - \delta\left(\xi + \frac{v_{dc}}{k}\right) \right] \\ &= \frac{1}{\text{Re } \tilde{j}_p(0)} \text{Im } \tilde{j}_{qp}\left(\frac{v_{dc}}{k}\right) \end{aligned}$$

or, using the definition of γ and $I_c \equiv (V_g/R_N)\text{Re } \tilde{j}_p(0)$, in physical units,

$$I(V_{dc}) = \frac{V_g}{R_N} \text{Im } \tilde{j}_{qp}\left(\frac{eV_{dc}}{\hbar\omega_g}\right). \tag{12}$$

Thus, at high values magnetic fields the IVC branches converge to the imaginary part of the quasiparticle tunnel current amplitude $\text{Im } \tilde{j}_{qp}$. Interestingly, expression (12) coincides with that for a voltage-biased small Josephson junction whose IVC is also given by $\text{Im } \tilde{j}_{qp}$.

5 Determination of the Riedel Peak Smearing from the IVC of FFO

The fact that the IVC branches at high magnetic field follow $\text{Im } \tilde{j}_{qp}$ can be used to extract value of the smoothing parameter from experimental data. In Fig. 2, we present our measurements of IVC of Nb–AlN–NbN FFO sample at high external magnetic field values. The experimental FFO sample was designed with a length $L = 400 \mu\text{m}$ and width profile $W(x) = 16 \mu\text{m}$ for $|x| < 160 \mu\text{m}$, decreasing linearly to $W(\pm L/2) = 1 \mu\text{m}$ at the edges as shown in Fig. 1. In the experimental setup, the external magnetic field h_{ext} was induced by the current in a dedicated control line I_{CL} taking a range of values as indicated in Fig. 2.

Note that in Fig. 2 the IVC branches condense into a single curve for $V \lesssim 0.9 \text{ mV}$. By comparing formula (12) to the experimental data for FFO IVC, we obtain an estimate for the smoothing parameter $\delta \approx 0.015$ and V_g/R_N ratio 0.55 A. In Fig. 2, theoretical dependences with $\delta = 0.005$ and $\delta = 0.025$ are also plotted for comparison. The apparent disagreement in the region above about 0.9 mV is caused by the fact that the experimental curves are measured in the current-biased regime with the bias current gradually increasing from zero. Thus, the experimental IVC curves exhibit a voltage jump where the theoretically predicted dependences reach a local maximum.

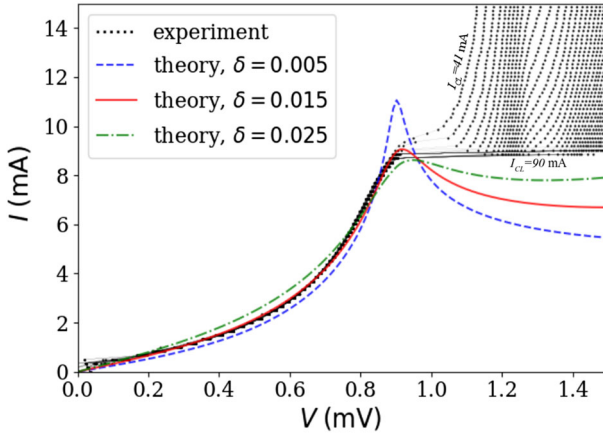


Fig. 2 Determination of Riedel peak smoothing parameter from the experimental IVC of FFO. Black dots represent experimental IVC curves of Nb–AlN–NbN FFO at high values of the external magnetic field: The magnetic field is induced by the current in the control line I_{CL} taking values in the range 41–90 mA with a step 1 mA. The red solid line represents theoretical IVC curve according to the formula (12) fitted to the experimental IVC curves at the smoothness parameter $\delta = 0.015$ and V_g/R_N ratio 0.55 A. For comparison, theoretical dependences at values $\delta = 0.005$ and $\delta = 0.025$ and the same value of V_g/R_N are also shown by dashed blue and green dashed-dotted lines (Color figure online)

6 Numerical Calculation of IVC of Nb–AlN–NbN FFO

We use the `MITMOJCO` C library [57,58] which implements the computationally efficient Odintsov–Semenov–Zorin algorithm [66] and serves to assist simulations of Josephson junctions based on the MTT. In our numerical simulations of FFO, we use the TCA calculated for Nb–AlN–NbN structure assuming 1.4 meV Nb gap, 2.3 mV NbN gap, temperature $T = 4.2$ K and the smoothing parameter $\delta = 0.015$ as estimated from the experiment as described in Sect. 5. For the TCAs to be used in numerical calculations with `MITMOJCO`, their fits by series of exponents need to be obtained. In our implementation of the fitting procedure, we follow Ref. [56]. First, the desired ratio τ_a/τ_r of the absolute τ_a and relative τ_r tolerances is chosen, which we take equal to 0.2. Then, we fit the exact TCAs by Fourier transforms of the sum of N exponentials [56,66] by minimizing the cost function

$$\sum_X \int_0^2 w(X^{\text{exact}}) (X^{\text{fit}} - X^{\text{exact}})^2 d\xi \tag{13}$$

using the least square routine. Here, X represents the functions $\text{Re } \tilde{j}_p(\xi)$, $\text{Im } \tilde{j}_p(\xi)$, $\text{Re } \tilde{j}_{qp}(\xi)$, $\text{Im } \tilde{j}_{qp}(\xi)$, respectively, and $w(X^{\text{exact}})$ is the weight function introduced to achieve a good fit of the TCA in the subgap region. Unfortunately, the improper behavior of the fitted TCA in the subgap region has been a major reason of failure of early attempts to employ the Odintsov–Semenov–Zorin algorithm to description of Josephson junctions [66–68]. Here, we take the weight function $w(X^{\text{exact}}) = 1/\max(\tau_a/\tau_r, |X^{\text{exact}}|)$ which stresses the low-valued regions of the TCAs. Fits of

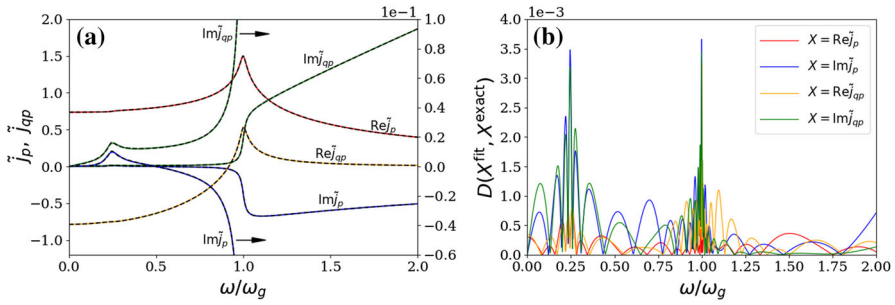


Fig. 3 **a** Dashed lines represent smoothed Bardeen–Cooper–Schrieffer (BCS) tunnel current amplitudes (TCAs) calculated for Nb–AlN–NbN junction assuming gap 1.4 meV for Nb and 2.3 meV for NbN, temperature $T = 4.2$ K, *after* the peak smoothing [Eqs. (7), (8)] with parameter $\delta = 0.015$ but *before* the supercurrent suppression [Eq. (9)]. Solid lines represent fits to the smoothed BCS TCAs in the form of the sum of exponentials [56,66] and are indistinguishable from the fits due to the high fit quality. Zoom by $20\times$ of the imaginary parts of the tunnel current amplitudes is shown to illustrate the adequate behavior of the fit in the subgap region. **b** Relative differences between the fitted and exact TCAs defined by Eq. (14) (Color figure online)

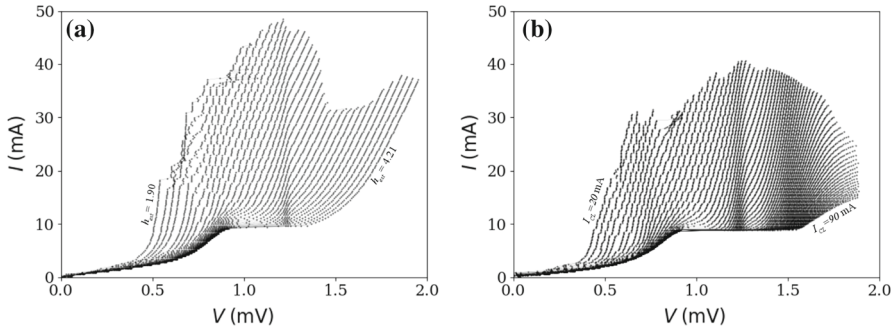


Fig. 4 **a** IVC of Nb–AlN–NbN FFO calculated numerically using the microscopic tunneling model implemented in MiTMoJCo code [57,58] and tunnel current amplitudes of Nb–AlN–NbN. The curves corresponds to different values of the external magnetic field h_{ext} in the range 1.90–4.21 with the step 0.07, in normalized units. **b** Experimental IVC of Nb–AlN–NbN FFO. The curves correspond to different values of the external magnetic field induced by the control current I_{CL} in the range 20–90 mA with the step 1 mA

TCAs obtained using $N = 8$ terms are shown in Fig. 3a. The exact TCAs are also shown by dashed lines, although these are indistinguishable from the fits due to the high fit quality. The relative errors defined as

$$D(X^{\text{fit}}, X^{\text{exact}}) \equiv \frac{|X^{\text{fit}} - X^{\text{exact}}|}{\max(\tau_a/\tau_r, |X^{\text{exact}}|)}. \tag{14}$$

are shown in Fig. 3b. As seen from the figure, our TCA fits achieve relative tolerance $\tau_r = 0.004$ at an absolute tolerance $\tau_a = 0.0008$.

Using the obtained TCA fits for Nb–AlN–NbN junction, we calculated numerically the IVC of Nb–AlN–NbN FFO using the MiTMoJCo code [57,58]. In our numerical calculations, we use the parameters $\lambda_J = 5.3 \mu\text{m}$, $k = 4.0$, $\alpha_{\text{supp}} = 0.7$, $\beta = 0.017$

and $V_g/R_N = 0.55$ A. Our results are shown in Fig. 4a. The experimental IVC is also provided for comparison in Fig. 4b. Numerically calculated IVC reflects the properties of the superconducting materials such information about their superconducting gaps. Similar to the experimental IVC, the numerical IVC curves at high magnetic field follow the imaginary part of the quasiparticle tunnel current according to the formula (12). At $V = (\Delta_{\text{NbN}} - \Delta_{\text{Nb}})/e$, the IVC curves exhibit a voltage step associated with the gap difference peak $\Delta_{\text{NbN}} - \Delta_{\text{Nb}}$ as in the experimental IVC. The numerical IVC captures well the signatures of self-coupling: At $V_g/3$ (1.23 mV), the curves exhibit a crossover associated with an increase in quasiparticle current via the photon-assisted tunneling. A higher-order crossover associated with two-photon absorption at $V_g/5$ (0.74 mV) can also be distinguished, although this seems to be less pronounced. There seems to be rather good agreement between the numerical and experimental IVCs in the region between 0.75 and 1.5 mV. However, discrepancies can be observed outside this region. At smaller voltages below about 0.75 mV, the experimental IVC exhibits well-pronounced Fiske steps which are not captured by our numerical model. At voltages about 1.5 mV, the IVC branches exhibit a cusp where the maximal flux-flow current (MFFC) values reach minimum. This turns out to be a universal feature which has been exhibited in numerical simulations of symmetric Nb–AlO_x–Nb junctions [56]. We could not explain these discrepancies within the present model and can attribute those to a possible influence of the idle region [69–77] which we neglect in the present model. The discrepancy for even higher voltages above 1.5 mV is associated with the influence of non-equilibrium effects which were also observed in Ref. [56] and cannot be described by the existing MTT which assumes the equilibrium distribution of quasiparticles [30].

7 Conclusion

Despite a number of theoretical works dedicated to the linewidth of flux-flow oscillators [36,38,42,43,47,49,52,53], the problem of an adequate theoretical description of FFO linewidth has not been solved: The experimentally observed linewidth and existing theoretical predictions still disagree by as much as order of magnitude. Given that the previous theoretical works were based on PSGE, such disagreement should not be surprising: For reliable theoretical treatment of FFO, the information about finite superconducting energy gaps of the materials should be necessarily taken into account which is ignored in PSGE. In this paper, we have introduced a theoretical description of Nb–AlN–NbN FFO based on the MTT. Our numerical model of Nb–AlN–NbN FFO captures the features of IVC associated with finite gaps of the superconductors: self-coupling and a voltage step at the gap difference voltage $(\Delta_{\text{NbN}} - \Delta_{\text{Nb}})/e$. The good agreement of our numerical model with experiments raises serious expectations that it may help to solve the longstanding problem of FFO linewidth.

The presented study uncovers the intrinsic limitation of MTT itself reflected in its inability to describe effects caused by non-equilibrium quasiparticle densities in the presence of radiation with frequencies above the Nb gap frequency. The disagreement between our experimental results and theoretical description in this frequency region

can be a motivating factor for theoretical developments beyond the currently existing equilibrium MTT.

We expect that the described microscopic approach to Nb–AlN–NbN junctions will be indispensable for theoretical description of Josephson systems of a non-trivial spatial layout containing a T-junction [78–81] implemented in Nb–AlN–NbN technology. Indeed, as shown in [82], presence of a T-junction may result in the appearance of the regime of chaotic self-coupling characterized by coupling of the tunnel currents to electromagnetic waves at all frequencies of a broad radiation spectrum rather than the Josephson frequency exclusively.

Acknowledgements The theoretical part of the work and numerical modeling are supported by the Russian Science Foundation under the Grant 18-12-00429. The experimental study is supported from the Grant No. 17-52-12051 of the Russian Foundation for Basic Research.

References

1. E.L. Wolf, G.B. Arnold, M.A. Gurvitch, J.F. Zasadzinski, *Josephson Junctions. History, Devices, and Applications* (Pan Stanford Publishing Pte. Ltd., Singapore, 2017)
2. J. Clarke, A.I. Braginski, *The SQUID Handbook Vol. I: Fundamentals and Technology of SQUIDS and SQUID Systems* (Wiley-VCH, Weinheim, 2004)
3. J. Clarke, A.I. Braginski, *The SQUID Handbook Vol. II: Applications of SQUIDS and SQUID Systems* (Wiley-VCH, Weinheim, 2006)
4. P. Seidel, *Applied Superconductivity: Handbook on Devices and Applications*, vol. 2 (Wiley-VCH, Weinheim, 2015)
5. S.K. Tolpygo, V. Bolkhovsky, T.J. Weir, L.M. Johnson, M.A. Gouker, W.D. Oliver, Fabrication process and properties of fully-planarized deep-submicron Nb/Al–AlO_x/Nb Josephson junctions for VLSI circuits. *IEEE Trans. Appl. Supercond.* **25**, 1101312 (2015)
6. S.K. Tolpygo, V. Bolkhovsky, T.J. Weir, A. Wynn, D.E. Oates, L.M. Johnson et al., Advanced fabrication processes for superconducting very large-scale integrated circuits. *IEEE Trans. Appl. Supercond.* **26**, 1100110 (2016)
7. R. Harris, *Phys. Rev. B* **81**, 134510 (2010)
8. M. Johnson et al., *Nature* **473**, 194–198 (2011)
9. A.M. Zagoskin, *Quantum Engineering: Theory and Design of Quantum Coherent Structures* (Cambridge University Press, Cambridge, 2011)
10. J.R. Tucker, *IEEE J. Quantum Electron.* **15**, 1234 (1979)
11. J.R. Tucker, M.J. Feldman, *Rev. Mod. Phys.* **57**, 1055 (1985)
12. A. Karpov, J. Blondell, M. Voss, K.H. Gundlach, Four photons sensitivity heterodyne detection of submillimeter radiation with superconducting tunnel junctions. *IEEE Trans. Appl. Supercond.* **5**, 3304 (1995)
13. A.M. Baryshev et al., *Astron. Astrophys.* **577**, A129 (2015)
14. J.M. Rowell, M. Gurvitch, J. Geerk, *Phys. Rev. B* **24**, 2278 (1981)
15. M. Gurvitch, W.A. Washington, H.A. Huggins, *Appl. Phys. Lett.* **42**, 472 (1983)
16. H.A. Huggins, M. Gurvitch, *J. Appl. Phys.* **57**, 2103 (1985)
17. T. Shiota, T. Imamura, S. Hasuo, *Appl. Phys. Lett.* **61**, 1228 (1992)
18. A.W. Kleinsasser, W.H. Mallison, R.E. Miller, *IEEE Trans. Appl. Supercond.* **5**, 2318 (1995)
19. J. Kawamura, D. Miller, J. Chen, J. Zmuidzinas, B. Bumble, H.G. Le Duc, J.A. Stern, *Appl. Phys. Lett.* **76**, 2119 (2000)
20. B. Bumble, H.G. LeDuc, J.A. Stern, K.G. Megerian, *IEEE Trans. Appl. Supercond.* **11**, 76 (2001)
21. N.N. Iosad, A.B. Ermakov, F.E. Meijer, B.D. Jackson, T.M. Klapwijk, *Supercond. Sci. Technol.* **15**, 945 (2002)
22. P.N. Dmitriev, I.L. Lapitskaya, L.V. Filippenko, A.B. Ermakov, S.V. Shitov, G.V. Prokopenko, S.A. Kovtonyuk, V.P. Koshelets, *IEEE Trans. Appl. Supercond.* **13**, 107 (2003)

23. MYu. Torgashin, V.P. Koshelets, P.N. Dmitriev, A.B. Ermakov, L.V. Filippenko, P.A. Yagoubov, *IEEE Trans. Appl. Supercond.* **17**, 379 (2007)
24. A. Khudchenko, A.M. Baryshev, K. Rudakov, V. Koshelets, P. Dmitriev, R. Hesper, L. de Jong, *IEEE Trans. Terahertz Sci. Technol.* **6**, 127 (2016)
25. T. Nagatsuma, K. Enpuku, F. Irie, K. Yoshida, *J. Appl. Phys.* **54**, 3302 (1983)
26. G. de Lange et al., *Supercond. Sci. Technol.* **23**, 045016 (2010)
27. V.P. Koshelets et al., *IEEE Trans. Terahertz Sci. Technol.* **5**, 687 (2015)
28. V.P. Koshelets, S.V. Shitov, A.V. Shchukin, L.V. Filippenko, J. Mygind, A.V. Ustinov, *Phys. Rev. B* **56**, 5572 (1997)
29. N.R. Werthamer, *Phys. Rev.* **147**, 255 (1966)
30. A.I. Larkin, YuN Ovchinnikov, *Sov. Phys. JETP* **24**, 1035 (1967)
31. V.P. Koshelets, S.V. Shitov, L.V. Filippenko, A.M. Baryshev, W. Luinge, H. Golstein, H. van de Stadt, J.-R. Gao, T. de Graauw, *IEEE Trans. Appl. Supercond.* **7**, 3589 (1997)
32. V.P. Koshelets, S.V. Shitov, *Supercond. Sci. Technol.* **13**, R53 (2000)
33. O. Kiselev, M. Birk, A. Ermakov, L. Filippenko, H. Golstein, R. Hoogeveen, N. Kinev, B. van Kuik, A. de Lange, G. de Lange, P. Yagoubov, V. Koshelets, *IEEE Trans. Appl. Supercond.* **21**, 612 (2011)
34. M. Li et al., *Phys. Rev. B* **86**, 060505 (2012)
35. C. Soriano, G. Costabile, R.D. Parmentier, *Supercond. Sci. Technol.* **9**, 578 (1996)
36. A.A. Golubov, B.A. Malomed, A.V. Ustinov, *Phys. Rev. B* **54**, 3047 (1996)
37. A.V. Ustinov, H. Kohlstedt, P. Henne, *Phys. Rev. Lett.* **77**, 3617 (1996)
38. A.P. Betenev, V.V. Kurin, *Phys. Rev. B* **56**, 7855 (1997)
39. M. Cirillo, N. Gronbech-Jensen, M.R. Samuelsen, M. Salerno, G.V. Rinati, *Phys. Rev. B* **58**, 12377 (1998)
40. M. Salerno, M.R. Samuelsen, *Phys. Rev. B* **59**, 14653 (1999)
41. M. Jaworski, *Phys. Rev. B* **60**, 7484 (1999)
42. M. Salerno, M.R. Samuelsen, A.V. Yulin, *Phys. Rev. Lett.* **86**, 5397 (2001)
43. A.L. Pankratov, *Phys. Rev. B* **65**, 054504 (2002)
44. A.L. Pankratov, *Phys. Rev. B* **66**, 134526 (2002)
45. A.S. Sobolev, A.L. Pankratov, J. Mygind, *Physica C* **435**, 112 (2006)
46. A.L. Pankratov, A.S. Sobolev, V.P. Koshelets, J. Mygind, *Phys. Rev. B* **75**, 184516 (2007)
47. A.L. Pankratov, V.L. Vaks, V.P. Koshelets, *J. Appl. Phys.* **102**, 063912 (2007)
48. M.M. Khapaev, M.Yu. Kupriyanov, *J. Phys.: Conf. Ser.* **129**, 012037 (2008)
49. A.L. Pankratov, *Phys. Rev. B* **78**, 024515 (2008)
50. A.L. Pankratov et al., *J. Phys.: Conf. Ser.* **97**, 012303 (2008)
51. M. Jaworski, *Phys. Rev. B* **81**, 224517 (2010)
52. E.A. Matrozova et al., *J. Appl. Phys.* **110**, 053922 (2011)
53. L.S. Revin, A.L. Pankratov, *Phys. Rev. B* **86**, 054501 (2012)
54. D.R. Gulevich, P.N. Dmitriev, V.P. Koshelets, F.V. Kusmartsev, *Nanosyst. Phys. Chem. Math.* **4**, 507 (2013)
55. K.K. Likharev, *Dynamics of Josephson Junctions and Circuits* (Gordon and Breach, New York, 1986)
56. D.R. Gulevich, V.P. Koshelets, F.V. Kusmartsev, *Phys. Rev. B* **96**, 024215 (2017)
57. Open source C library MiTMOJCo (Microscopic Tunneling Model for Josephson Contacts), <https://github.com/drgulevich/mitmojco>
58. D.R. Gulevich, MiTMOJCo: Microscopic Tunneling Model for Josephson Contacts, [arXiv:1809.04706](https://arxiv.org/abs/1809.04706)
59. M. Khapaev, *IEEE Trans. Microw. Theory Tech.* **49**, 217 (2001)
60. M.M. Khapaev, MYu. Kupriyanov, *J. Phys.: Conf. Ser.* **248**, 012041 (2010)
61. M.M. Khapaev, MYu. Kupriyanov, *Supercond. Sci. Technol.* **28**, 055013 (2015)
62. E.H. Rhoderick, E.M. Wilson, *Nature (London)* **194**, 1167 (1962)
63. R.E. Harris, *Phys. Rev. B* **11**, 3329 (1975)
64. A.B. Zorin, I.O. Kulik, K.K. Likharev, J.R. Schrieffer, *Sov. J. Low Temp. Phys.* **5**, 537 (1979)
65. D.K. Finnemore, T.F. Stromberg, C.A. Swenson, *Phys. Rev.* **149**, 231 (1966)
66. A.A. Odintsov, V.K. Semenov, A.B. Zorin, *IEEE Trans. Magn.* **23**, 763 (1987)
67. N. Gronbech-Jensen, S.A. Hattel, M.R. Samuelsen, *Phys. Rev. B* **45**, 12457 (1992)
68. S.A. Hattel, N. Gronbech-Jensen, M.R. Samuelsen, *Phys. Lett. A* **178**, 150 (1993)
69. G.S. Lee, *IEEE Trans. Appl. Supercond.* **1**, 121 (1991)
70. G.S. Lee, A.T. Barfknecht, *IEEE Trans. Appl. Supercond.* **2**, 67 (1992)
71. J.-G. Caputo, N. Flytzanis, M. Devoret, *Phys. Rev. B* **50**, 6471 (1994)

72. R. Monaco, G. Costabile, N. Martucciello, *J. Appl. Phys.* **77**, 2073 (1995)
73. N. Thyssen, A.V. Ustinov, H. Kohlstedt, S. Pagano, J.-G. Caputo, N. Flytzanis, *IEEE Trans. Appl. Supercond.* **5**, 2965 (1995)
74. J.-G. Caputo, N. Flytzanis, E. Vavalis, *Int. J. Mod. Phys. C* **07**, 191 (1996)
75. J.-G. Caputo, N. Flytzanis, V. Kurin, N. Lazarides, E. Vavalis, *J. Appl. Phys.* **85**, 7291 (1999)
76. A. Franz, A. Wallraff, A.V. Ustinov, *J. Appl. Phys.* **89**, 471 (2001)
77. A. Benabdallah, J.-G. Caputo, *J. Appl. Phys.* **92**, 3853 (2002)
78. D.R. Gulevich, F.V. Kusmartsev, *Phys. Rev. Lett.* **97**, 017004 (2006)
79. D.R. Gulevich, F.V. Kusmartsev, *Supercond. Sci. Tech.* **20**, S60 (2007)
80. D.R. Gulevich, F.V. Kusmartsev, *New J. Phys.* **9**, 59 (2007)
81. D.R. Gulevich, M. Gaifullin, O.E. Kusmartseva, F.V. Kusmartsev, K. Hirata, *Physica C* **468**, 1903 (2008)
82. D.R. Gulevich, V.P. Koshelets, F.V. Kusmartsev, Bridging the Terahertz gap for chaotic sources with superconducting junctions, [arXiv:1709.04052](https://arxiv.org/abs/1709.04052)